JOURNAL OF AIRCRAFT
Vol. 48, No. 1, January–February 2011

Behavior of Detached-Eddy Simulations for Mild Airfoil Trailing-Edge Separation

Naveed Durrani* and Ning Qin†
University of Sheffield, Sheffield, England S1 3JD, United Kingdom

DOI: 10.2514/1.C031058

The flow around the A-airfoil at the maximum lift condition ($\alpha = 13.3°$) with a chord Reynolds number of 2×10^6 is simulated using unsteady Reynolds-averaged Navier–Stokes solution, detached-eddy simulation, and delayed-detached eddy simulation. This case features a relatively thick boundary layer with a mild trailing-edge separation. Detailed comparisons of the modeled Reynolds stresses are carried out with the available experimental data at different locations on the suction side of the airfoil and in the wake region. The impact of the delayed switching on modeled Reynolds stresses from delayed-detached-eddy simulation as compared with the original detached-eddy simulation is studied. On the suction side of the airfoil, the modeled turbulent Reynolds stresses computed through the detached-eddy simulation are generally lower than the unsteady Reynolds-averaged Navier–Stokes solutions, whereas the delayed-detached-eddy simulation gives comparable values with the unsteady Reynolds-averaged Navier–Stokes solutions results. None of them give consistent comparison with the experimental Reynolds stresses. It is observed that for the cases with the mild separation, the original detached-eddy simulation may perform better than the delayed-detached-eddy simulation, due to its relatively lower turbulent dissipation levels. The detached-eddy simulation Reynolds stresses in the wake region show better results, in comparison with the experimental data.

Nomenclature

A	=	surface area
C_{DES}	=	model constant taken as 0.65
C_d	=	drag coefficient
C_l	=	lift coefficient
c	=	chord length
d	=	wall distance, length scale for turbulence model
dA	=	differential surface area
$E(k)$	=	energy contained by length scales
$\mathbf{F}$	=	inviscid fluxes
$\mathbf{G}$	=	viscous fluxes
M	=	Mach number
n	=	normal area vector
P, p	=	pressure
$\mathbf{Q}$	=	primitive variable vector
R	=	gas constant
Re	=	Reynolds number
S	=	strain-rate tensor
T	=	temperature
t	=	time
U_{inf}	=	freestream velocity
U_r	=	reference velocity
u	=	instantaneous velocity
$\bar{u}$	=	averaged velocity
u, v, w	=	Cartesian velocity components
V	=	volume
$\mathbf{W}$	=	conservative variable vector
$\mathbf{\Gamma}$	=	Jacobian matrix
γ	=	ratio of specific heats
Δ	=	local grid spacing
η	=	spanwise location
μ	=	molecular viscosity
μ_T	=	turbulent or eddy viscosity
μ_0	=	μ at reference state
$\tilde{\nu}$	=	modified kinematic eddy viscosity
ν_T	=	kinematic eddy viscosity
ρ	=	density
ρ_p	=	$\partial\rho/\partial p$ at constant temperature
ρ_T	=	$\partial\rho/\partial T$ at constant pressure
ρ'	=	instantaneous fluctuation term in Reynolds-averaging
$\boldsymbol{\tau}$	=	stress tensor, $[\tau_{ij}]$
τ	=	pseudotime
τ_w	=	wall shear stress
Ω	=	rotation rate tensor
∇	=	gradient, increment
$\bar{\ }$	=	time-averaged quantity
$\langle\,\rangle$	=	time-averaged quantity
$'$	=	fluctuating quantity

Introduction

SEPARATED flows around airborne objects such as an aircraft are an important and challenging area of study for aerodynamic applications. Computational power is a severe limitation if high-order physical simulation techniques such as large-eddy simulation (LES) [1,2] or direct numerical simulation [3,4] are applied to numerically simulate these flows, as pointed out in [2,3]. Whereas the results from computationally feasible Reynolds-averaged Navier–Stokes (RANS) scheme have difficulties in modeling separated flows, hybrid RANS-LES schemes such as detached-eddy simulation (DES) [5] have become a promising choice for practical applications. The ability to capture separated flows with affordable computational cost has prompted their use over a wide range of application areas, especially for flows with massive separation. The main theme of the DES scheme is to combine the strengths of the RANS scheme near the solid wall boundaries and LES elsewhere. The natural implementation was intended to simulate the entire boundary layer using the RANS scheme and the separated region with the LES scheme. However, a shortcoming in the original DES was pointed out by Menter and Kuntz [6], suggesting that a blending function may be used in order to avoid a premature switching within the boundary-layer region from RANS to LES. This premature switching is caused by excessive mesh clustering, either near the trailing edge or in thick boundary layers. To overcome such

Received 8 April 2010; revision received 2 July 2010; accepted for publication 29 September 2010.

*Postgraduate Student, Department of Mechanical Engineering. Member AIAA.

†Professor of Aerodynamics, Department of Mechanical Engineering. Associate Fellow AIAA.

problems, a modified version of DES, named delayed detached-eddy simulation (DDES) was proposed in [7]. A detailed review of the DES technique with the perspective of its applications and ensuing promising results were presented in [8], with further references within.

The fundamental computational limitation of LES scheme is the requirement of near-wall mesh resolution in wall-normal, wall-tangential, and spanwise directions for high Reynolds number flows. It drastically increases the mesh size and, in turn, the associated computational cost in comparison with the RANS approach. On the other hand, RANS only requires the relatively high mesh resolution in the wall-normal direction. Although it reduces the computational cost considerably, the accuracy of the solution for the separated flows is not generally satisfactory. DES using RANS in the near-wall region and LES in the separated region leads to a basic question about the accuracy of the resulting solution notably in turbulence parameters being computed. With the acceptance of the Boussinesq hypothesis in solving the closure problem using turbulence modeling, it is very important to quantify and compare the resulting Reynolds stresses with the known experimental data to judge the appropriateness of the simulation technique in terms of the turbulence parameters. However, the availability of the experimental data for Reynolds stresses is rather limited in the open literature. A European initiative to assess the feasibility of using LES for calculating the flow around airfoils was reported [9–11]. Detailed experimental data, including the Reynolds stresses, were made available for flow around the Aérospatiale A-airfoil at different angles of attack and at high Reynolds numbers.

The work presented contains the computational fluid dynamics simulations of the flow over the Aérospatiale A-airfoil at an angle of attack of 13.3° (maximum lift condition) with a chord based Reynolds number of 2×10^6 and at a subsonic Mach number of 0.15. Typically this is a high-lift condition near stall. The experimental data from the wind tunnel [12] are used for comparison. It contains data for velocity profiles and Reynolds stresses at different wall-normal and streamwise directions after the transition point ($x/c \geq 0.3$). The simulation techniques used are URANS, DES, and DDES. One of the main objectives of this study is to compare the relative performance of DES and its modified formulation DDES, for the mildly separated flows, along with the URANS approach with turbulence modeling.

Various numerical studies were carried out and reported by the partners [2,9,13] of LESFOIL and other research groups [14]. Results of these numerical studies were compiled and discussed in [10,11]. As noted, from the point of view of flow separation on the suction side at the trailing edge, this flow is much more difficult to predict than a situation involving massive separation at higher angles of attack or where separation occurs from a sharp edge. The results from various studies in [10] were contradictory regarding the prediction of the trailing-edge separation: some did and others did not. Another observation mentioned in [10] is that the C_f plot of results from some partner fails to show the separation, although it is observed in the streamline plots. Results presented by Schmidt and Thiele [14] show the flow around the A-airfoil and the modeled, as well as the resolved, Reynolds stresses for some of the stations of the given data. The RANS solution predicts the separation, but fails to show the transient vortex shedding, whereas the LES solution predicts the transient vortex shedding.

Numerical Scheme

The Dynamic-Grid Detached Eddy Simulation (DG-DES) [15,16] code is an in-house-developed code and it can simulate moving and nonmoving wall cases using RANS, DES, and DDES. The flow governing equations are discretized using a cell-centered finite volume method. A one-equation Spalart–Allmaras turbulence model [17] is used for the detached-eddy simulation formulation. Further details can be found in [18,19]. The convective terms are discretized using the Roe scheme [20]. METIS,[‡] an open-source program, is used for the mesh partitioning in the DG-DES code for parallel computing. The second-order spatial accuracy is obtained with the piecewise linear reconstruction of the flow variables.

[‡]Data available online at http://glaros.dtc.umn.edu/gkhome/views/metis [retrieved 2010].

Dual-Time-Stepping

$$\underbrace{\frac{\partial}{\partial t}\iiint_V \mathbf{W}\,\mathrm{d}V}_{\text{physical time term}} + \underbrace{\Gamma\frac{\partial}{\partial \tau}\iiint_V \mathbf{Q}\,\mathrm{d}V}_{\text{pseudotime term}} = -\iint_A [\mathbf{F}-\mathbf{G}]\,\mathrm{d}\mathbf{A} \qquad (1)$$

where $\mathbf{W}$ is the conservative variable vector, $\mathbf{Q}$ is the primitive variable vector, $\mathbf{F}$ and $\mathbf{G}$ are inviscid and viscous fluxes, and Γ is the conjugate $\partial\mathbf{W}/\partial\mathbf{Q}$.

A dual-time-stepping approach is used as described in Eq. (1) and is similar to the formulation used in [21]. The essential idea of the dual-time-stepping approach is to add an extra unsteady term to the original Navier–Stokes equation as a pseudotime term represented by τ, as shown in Eq. (1). Dual-time-stepping permits various schemes, including the explicit multistage Runge–Kutta method, to be used with an implicit physical temporal discretization. The convergence of the solution in pseudotime is sought to obtain the solution at the present physical time level. It is evident that as the pseudotime iteration converges, the second term in Eq. (1) vanishes and the temporal accuracy of the solution depends on the first term representing the physical time only. The low-Mach-number preconditioning and artificial compressibility are combined in a way to enhance the convergence rates of the density-based time-marching schemes for solving flows at all speeds. It is able to accurately simulate unsteady flows with integrated dual-time-stepping, as shown in [21,22].

Detached-Eddy Simulation

The DES approach was proposed by Spalart et al. in 1997 [5]. The main theme of the DES scheme was to combine the strengths of the RANS scheme near the solid wall boundaries and LES elsewhere. The original DES proposed combines the RANS and LES in a nonzonal manner, based on the Spalart–Allmaras (S-A) one-equation turbulence model [17]. The model's length scale d, generally taken as the shortest distance at any point to the closest wall in RANS mode, is replaced with the minimum between the distance to the wall and a length proportional to the local grid spacing. It is represented mathematically as

$$d_{\mathrm{DES}} = \min(d, C_{\mathrm{DES}}\Delta) \qquad (2)$$

where C_{DES} represents a model constant taken as 0.65 in various studies [18], and Δ is the local grid spacing. For structured grids, it is the maximum grid spacing over all three directions. In the boundary-layer regions near the wall, Δ far exceeds the distance to the wall, d, and the standard Spalart–Allmaras RANS turbulence model [17] is recovered. However, away from the boundaries, the distance to the closest wall exceeds $C_{\mathrm{DES}}\Delta$, and the model becomes a simple one-equation subgrid-scale model for LES with the model length scale proportional to the grid spacing.

Delayed-Detached-Eddy Simulation

The original DES, known as DES97, has an inherent shortcoming of switching from RANS to LES mode within the boundary layer for relatively thick boundary layers or at locations with increased grid density: e.g., near the leading or trailing edge of an airfoil. This problem was highlighted by Menter and Kuntz [6] in their study of Ahmad's car model.

Spalart et al. [19] proposed a new version of DES (DDES) to tackle this problem. The main idea of DDES is to include the molecular and turbulent viscosity information into the switching mechanism to delay this switching in boundary layers. The length scale is redefined as

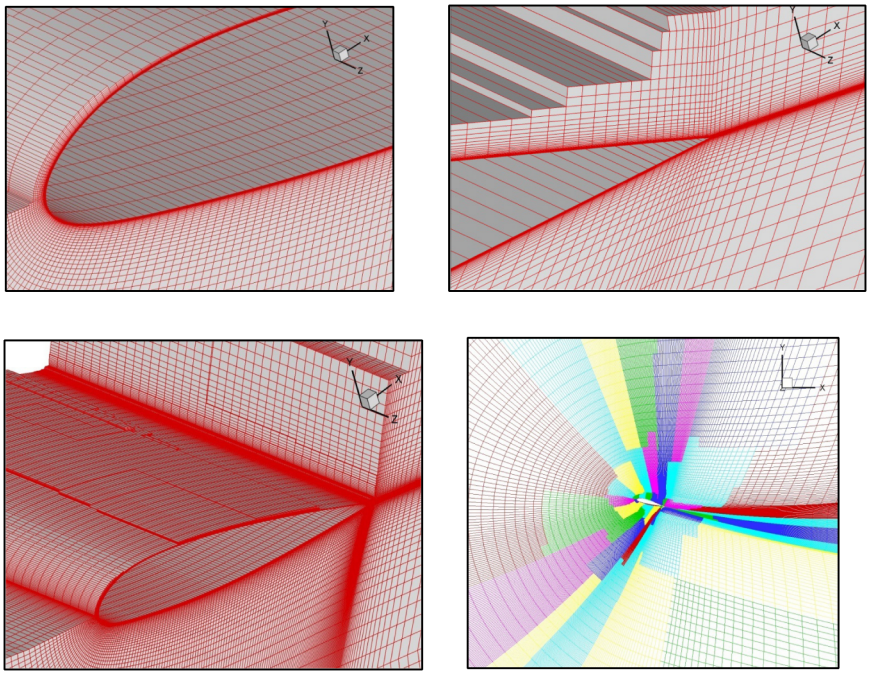

Fig. 1 Mesh around the Aérospatiale A-airfoil: zoomed view at leading edge (top left), zoomed view at the trailing edge (top right), broken view (bottom left), and mesh with 120 partitions with each partition represented with different shade (bottom right).

$$\tilde{d} \equiv d - f_d \max(0, d - C_{\mathrm{DES}}\Delta) \tag{3}$$

$$f_d \equiv 1 - \tanh([8r_d]^3) \tag{4}$$

$$r_d \equiv \frac{\nu_t + \nu}{\sqrt{U_{i,j}U_{i,j}\kappa^2 d^2}} \tag{5}$$

In the present study, the RANS, DES, and DDES are all run in fully turbulent mode and hence no transition tripping is used. The effect of switching to LES mode and its delay will have the major impact in the flow simulation.

Geometry

The wind-tunnel model used in the experiments has a very small blunted trailing edge. Mellen [10] described the different studies carried out to investigate the effect of approximating this with a sharp trailing edge and concluded that no change was found in the flow statistics due to this geometric simplification. The sharp trailing-edge geometry is therefore used in this study.

Computational Mesh

The mesh was created using a commercial grid generation software, Gambit, as shown in Fig. 1. To achieve a good boundary-layer resolution in the wall-normal direction, the first cell normal to the wall was placed at $6 \times 10^{-6}c$ giving an overall wall Δy^+ less than one on the airfoil. The computational flow domain extends $9c$ and $12c$ from the airfoil leading and trailing edges up and downstream, respectively. The top and bottom far-field boundaries are $8c$ from the airfoil surface. The mesh details are listed in Table 1.

The mesh size is very coarse as compared with what is generally required in LES to simulate an airfoil wing. The wall-normal direction resolution in the near-wall region is suited for the turbulence modeling in the RANS solution with very-high-aspect-ratio cells. N_z represents the number of cells along span and L_z is the spanwise dimension of the simulation domain.

Symmetry boundary conditions are used for the side walls on either side in the spanwise direction. Characteristic boundary conditions are used as far-field boundary conditions for the outer boundary.

Results

First, the first cell Δy^+ distribution was investigated to make sure that in the RANS mode the turbulence boundary layer is resolved by the turbulence model. Typical Δy^+ for all the simulations was less than one over the complete A-airfoil, as shown in Fig. 2.

This not only provides better resolution in wall-normal direction as required by RANS, but also is important for the convergence of the S-A turbulence model in the simulations.

Figure 3 shows the time-averaged velocity contour plots and the streamlines near the trailing edge for the A-airfoil from DES and DDES, respectively. The DES solution shows the separation in the flow in the trailing-edge region, whereas the DDES solution, similar to URANS, failed to predict any separation. The reason is that the DDES scheme, due to the delay in switching from RANS to LES mode, causes excessive turbulent dissipation in the flow by extending the RANS region. Consequently, it damps the unsteadiness in the flow, and the DDES solution appears very similar to the URANS solution.

To understand it better, the differences in surface pressure computed by using the URANS, DES, and DDES are compared with the available experimental data [12]. The surface pressure plot C_p in Fig. 4, including zoomed views near the leading edge, shows that the initial dip in DES and overshoot of URANS are balanced by the DDES results. It means that the early switching of DES in the leading-edge section is the main cause of lower C_p values.

The results indicate that the effect of switching to LES mode and its delay have a major impact in the flow simulated. Figure 5 shows

Table 1 Mesh details for the A-airfoil

Statistics	Values
Mesh size	
Type	Structured
Cells	1,936,000
Nodes	2,004,080
Mesh quality	
N_z	40
L_z/c	0.25
x^+	20–950
y^+	<1
z^+	100–600

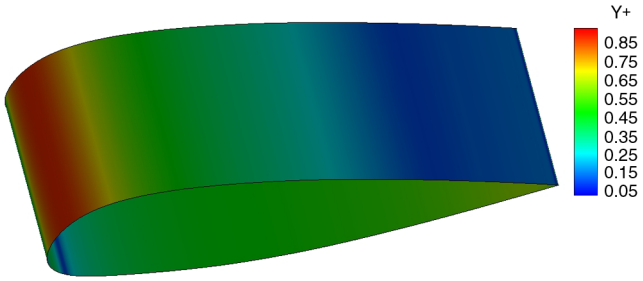

Fig. 2 Δy^+ values on the Aérospatiale A-airfoil.

that the RANS region (near wall) and LES region (away from wall) are quite different for DES and DDES schemes, impacting on the pressure distribution and skin-friction coefficient results from the respective schemes. The switching regions, as shown in Fig. 5, have a strong impact on the solution dissipation and result in different flow pictures for different schemes. It clearly shows that, for DES, part of the attached boundary layer is actually simulated with LES, in addition to the trailing-edge mild separated region.

It is interesting to observe the switching regions to URANS and LES modes by DES and DDES schemes, as shown in Fig. 5. DDES region at the suction side near the trailing edge is thicker and follows the trend of the thicker boundary layer with a delay in the switching to

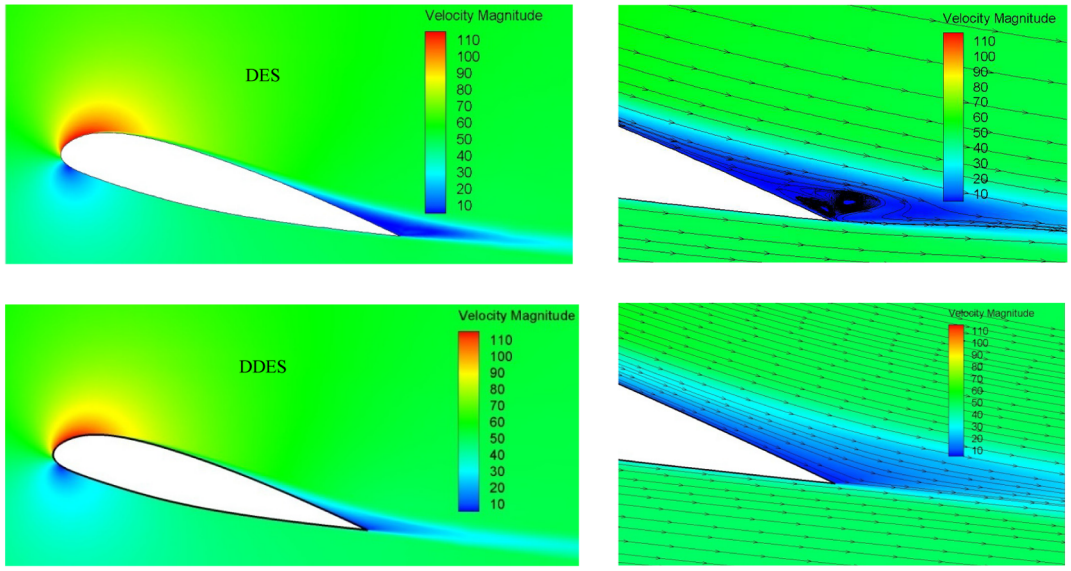

Fig. 3 Time-averaged velocity magnitude contour for DES (top) and DDES (bottom) with zoomed views near the trailing edge with time-averaged streamlines (left).

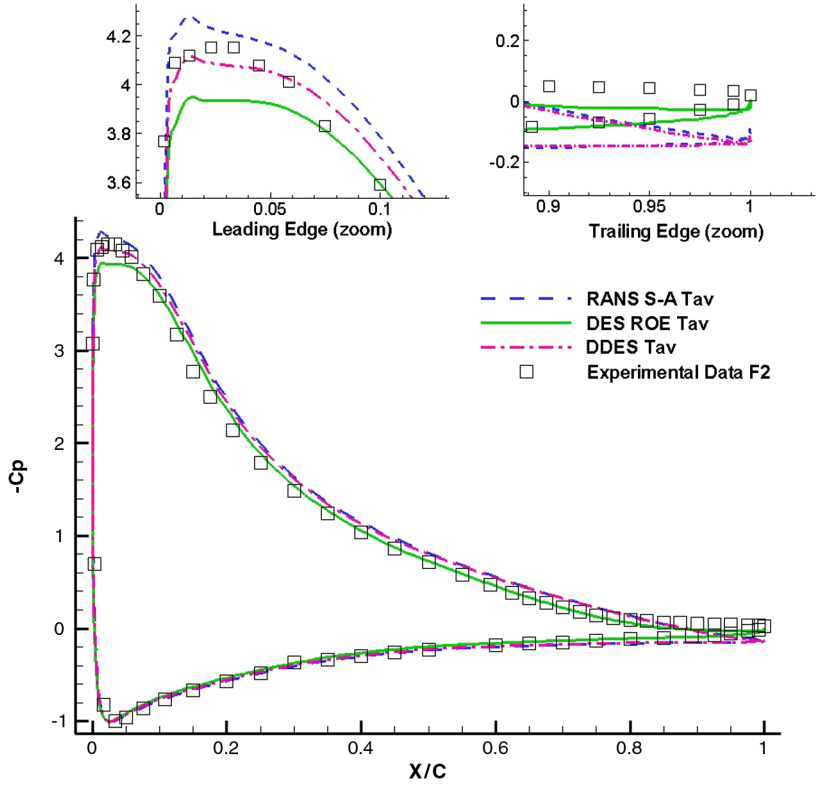

Fig. 4 Comparison of computed time-averaged (Tav) pressure coefficient from RANS, DES, and DDES on Aérospatiale A-airfoil with experimental data.

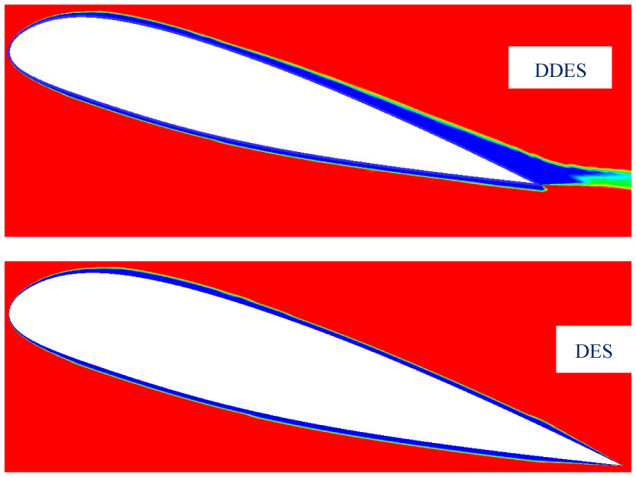

Fig. 5 LES and URANS (near-wall) region bifurcation used in the DDES (top) and DES (bottom) simulations.

the LES mode as intended. It increases the dissipation in the flow causing the separation region predicted by the DES to disappear. There is a strong similarity between the URANS and DDES results, due to the delay in switching for the DDES. DDES, in effect, modeled most of the boundary layer as URANS, showing the same problem of incapability to predict trailing-edge separation.

The skin-friction coefficient C_f distributions from URANS, DES, and DDES are compared in Fig. 6. There are only very minor differences between URANS and DDES. The most significant difference is in the trailing-edge region between DES and the other two; none give negative surface friction. Referring back to Fig. 3, the trailing-edge separation is captured in DES. However, it is neither a normal separation bubble near the leading edge nor a long bubble around the midchord. At the trailing edge, a counter rotating (anticlockwise) vortex separated from the trailing-edge point is formed underneath the primary trailing-edge separation (clockwise). It pushes the primary separation vortex upward and results in positive skin friction on the upper surface near the trailing edge. This trailing-edge separation with positive skin friction was also observed in some other simulations in [10]. This simulated phenomenon contradicts the negative skin friction in the experimental data.

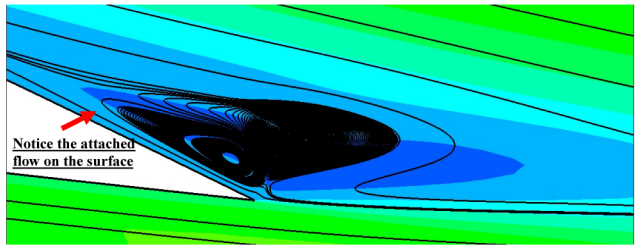

a)

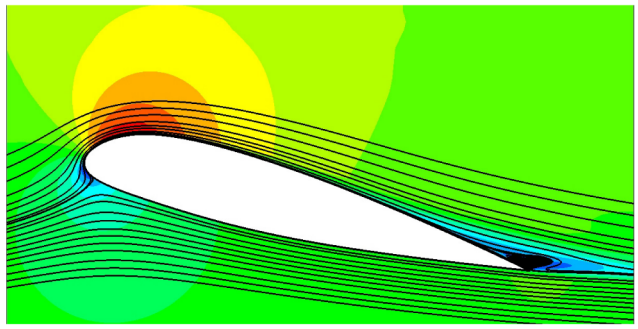

b)

Fig. 7 DES streamlines on A-airfoil with pressure contours (bottom) and zoom view of separation with streamlines (top). (Note that the separation is not on the surface.)

The impact of switching is further augmented by Fig. 6, which shows that the skin friction has increased to a similar level to that of URANS. Further downstream, due to the presence of the thick boundary layer, the DDES solution closely follows URANS, in contrast with DES. This is logical, because the solution of DDES in attached boundary layers is the same as URANS, since no switching from RANS to LES has been done within the boundary layer.

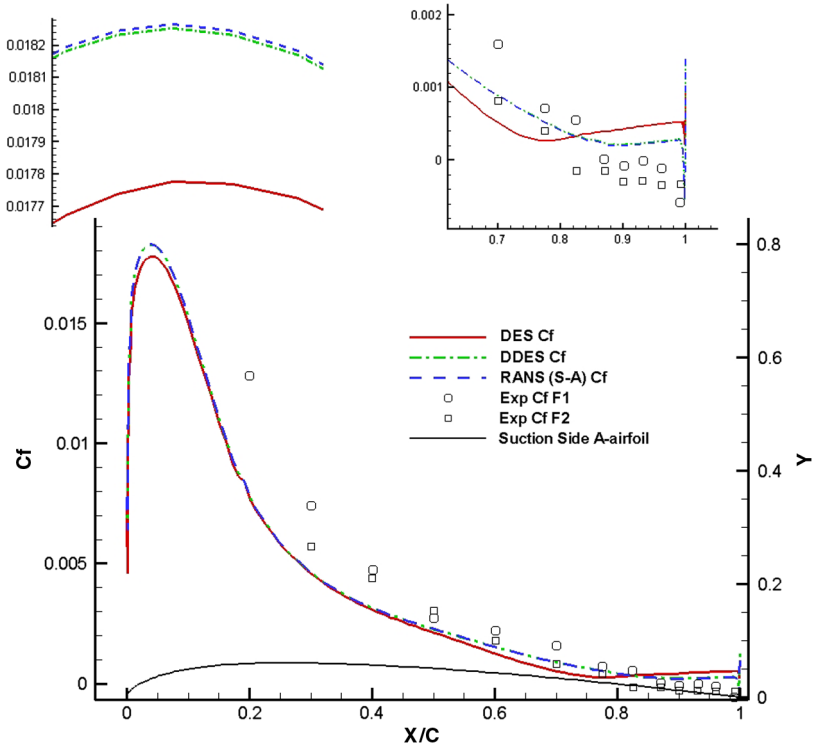

Fig. 6 Comparison of skin-friction coefficient C_f from RANS, DES, and DDES on suction side of Aérospatiale A-airfoil with suction-side profile. Zoomed leading and trailing edge on top.

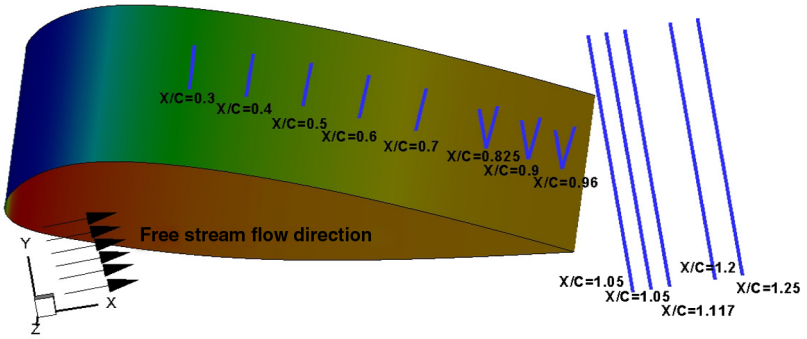

Fig. 8 A-airfoil with probe orientation on surface and wake region for data extraction. Surface is shaded by static pressure. Flow direction is in $+x$-axis direction.

The disparity between URANS and DDES arises when the DDES switches from URANS to LES, thus lowering the turbulent dissipation.

To study this further, streamlines were plotted around the A-airfoil surface, as shown in Fig. 7. The zoomed view of at the suction side of the trailing edge shows that the flow is attached on the surface and the separation region is actually aft of the suction-side surface. For this reason, the C_f plot does not depict any dip or becomes negative in this region. The mesh used in the computation is very fine in the near-wall region to satisfy the RANS requirements, and its Δy^+ value is less than 1. This Δy^+ value should be sufficient to compute the solution with good accuracy from mesh density perspective for RANS. Similarly, the Δx^+ and Δz^+ are also in reasonable range as compared with the other studies reported in [10].

It was observed that both URANS and DDES do not show any unsteadiness in the flow. Only DES results show the unsteadiness in the flow at the trailing edge. However, it does not show any transient vortex shedding as reported in some previous work. Resolved stresses were not computed, with the view that no significant values will be obtained as an output, due to mostly steady flowfields.

Modeled Turbulent Reynolds Stresses

The Boussinesq hypothesis provided a solution for the turbulence closure. This approximation assumes that the turbulence stresses are directly proportional to the velocity gradient, with eddy viscosity (μ_t) as the constant of proportionality. This value can be further modeled using different turbulence models.

From the Boussinesq hypothesis [3,23], the eddy viscosity is linearly related to the Reynolds turbulent stresses. The assumption of μ_t as an isotropic scalar quantity in the Boussinesq hypothesis may not be strictly true. However, the alternate option is to go for more computationally expensive Reynolds stress transport equations. The S-A model used in this study uses the Boussinesq hypothesis.

The basic relationship is drawn from analogy with molecular transport of momentum:

$$\overline{u_i' u_j'} = \frac{2}{3}(k)\delta_{ij} - \nu_t\left(\frac{\partial U_i}{\partial x_j} + \frac{\partial U_j}{\partial x_i}\right) \tag{6}$$

It provides the following normal and shear stress components for Reynolds stresses:

$$\overline{u'u'} = \frac{2}{3}(k) - \nu_t\left(\frac{\partial U}{\partial x} + \frac{\partial U}{\partial x}\right) \qquad \overline{v'v'} = \frac{2}{3}(k) - \nu_t\left(\frac{\partial V}{\partial y} + \frac{\partial V}{\partial y}\right)$$
$$\overline{u'v'} = -\nu_t\left(\frac{\partial U}{\partial y} + \frac{\partial V}{\partial x}\right) \tag{7}$$

where U and V are the mean velocity components. For two-equation turbulence models using turbulent kinetic energy k as a variable in the equation, k is calculated from solution of those equations. However, in the one-equation S-A turbulence model, k is not explicitly calculated. Hence, it is to be approximated using Bradshaw's hypothesis [24].

The turbulent energy equation for a two-dimensional incompressible mean flow, outside the viscous sublayer, is given in [25] as

$$q^2 = u'^2 + v'^2 + w'^2 = 2k \qquad \tau = -\rho\overline{u'v'} \tag{8}$$

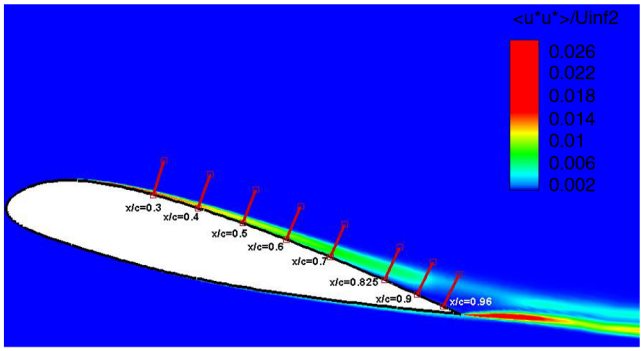

a)

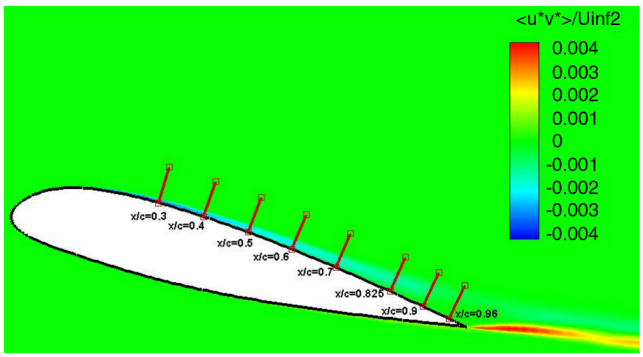

b)

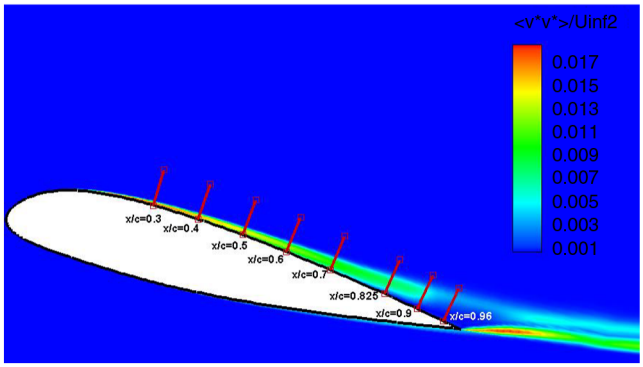

c)

Fig. 9 Contour plots of the modeled turbulent Reynolds stresses form DES simulation normalized by the square of the inlet velocity with probes for normal to the surface data extraction.

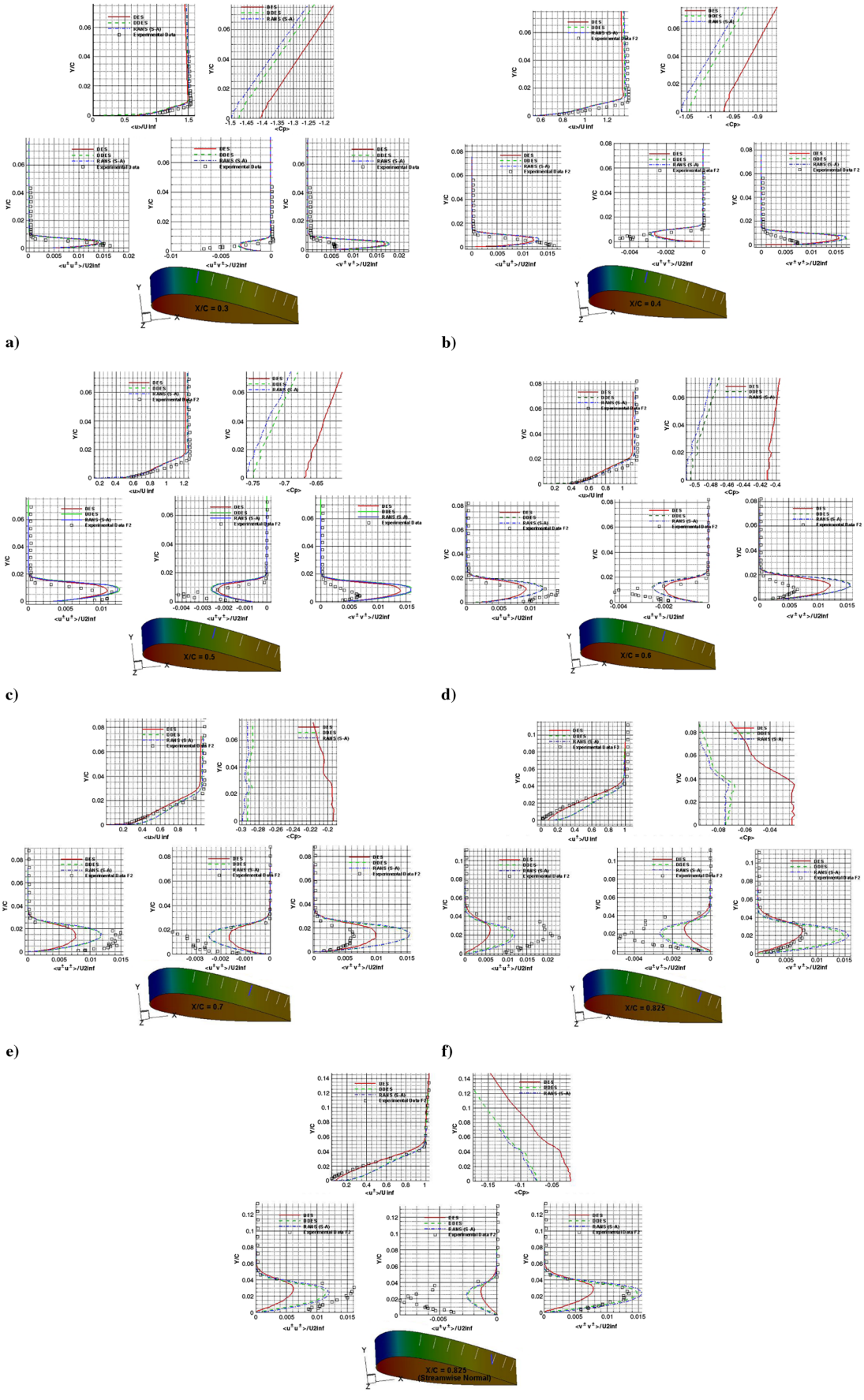

Fig. 10 Comparison of $\langle u \rangle$, modeled Reynolds stresses, and $\langle C_p \rangle$ from RANS, DES, and DDES with experimental data F2: a–f) computed normal to the airfoil surface and g) computed normal to the freestream flow direction at the specified location.

$$\underbrace{\frac{1}{2}\rho\left(U\frac{\overline{\partial q^2}}{\partial x}+V\frac{\overline{\partial q^2}}{\partial y}\right)}_{\text{advection}}-\underbrace{\tau\frac{\partial U}{\partial y}}_{\text{production}}$$
$$+\underbrace{\frac{\partial}{\partial y}\left(\overline{pv}+\frac{1}{2}\rho\overline{q^2v}\right)}_{\text{diffusion}}+\underbrace{\rho\varepsilon}_{\text{dissipation}}=0 \qquad (9)$$

and

$$\varepsilon=\upsilon\left(\frac{\partial u_i}{\partial x_j}\right)^2$$

It can be regarded as an equation for the advection or rate of change of turbulent kinetic energy along a mean streamline through a point if all the other terms are known at that point.

Defining

$$a1\equiv\frac{\tau}{\rho\bar{q}^2} \qquad L\equiv\frac{(\tau/\rho)^{3/2}}{\varepsilon} \qquad G\equiv\frac{((\overline{pv}/\rho)+\frac{1}{2}\overline{q^2v})}{(\tau_{\max}/\rho)^{1/2}(\tau/\rho)}$$

The choice of empirical function gives [24]

$$a1=\frac{-\rho\overline{uv}}{\rho(\bar{u}'^2\bar{v}'^2+\bar{w}'^2)} \qquad a1=\frac{\tau}{\frac{1}{2}\rho\bar{q}^2}=0.3 \qquad a1=\frac{\tau}{k}=0.3$$

Considering a 2-D log-law boundary layer, put

$$a1=\sqrt{C_\mu}(\Rightarrow C_\mu=0.09)$$

$$\frac{\tau}{k}=\sqrt{C_\mu}$$

$$k=\frac{\tau}{\sqrt{C_\mu}} \quad \therefore \tau=-\rho\overline{uv}$$

It can be further elaborated as

$$k=\frac{\nu_t\left|\frac{\partial u}{\partial y}\right|}{\sqrt{C_\mu}}=\frac{\nu_t S^*}{\sqrt{C_\mu}} \quad \therefore S^*=\sqrt{2S_{ij}S_{ij}} \qquad S_{ij}=\frac{1}{2}\left(\frac{\partial U_i}{\partial x_j}+\frac{\partial U_j}{\partial x_i}\right) \qquad (10)$$

Similar approximations for k have been used in [26]. In the experimental setup F2 for the Aérospatiale A-airfoil, the data were extracted along different spanwise and streamwise stations. It also contains the wake data at different stations for the wake flow analysis. The probe lines along streamwise directions on the suction side and in the wake region with their respective lengths and locations are presented in Fig. 8.

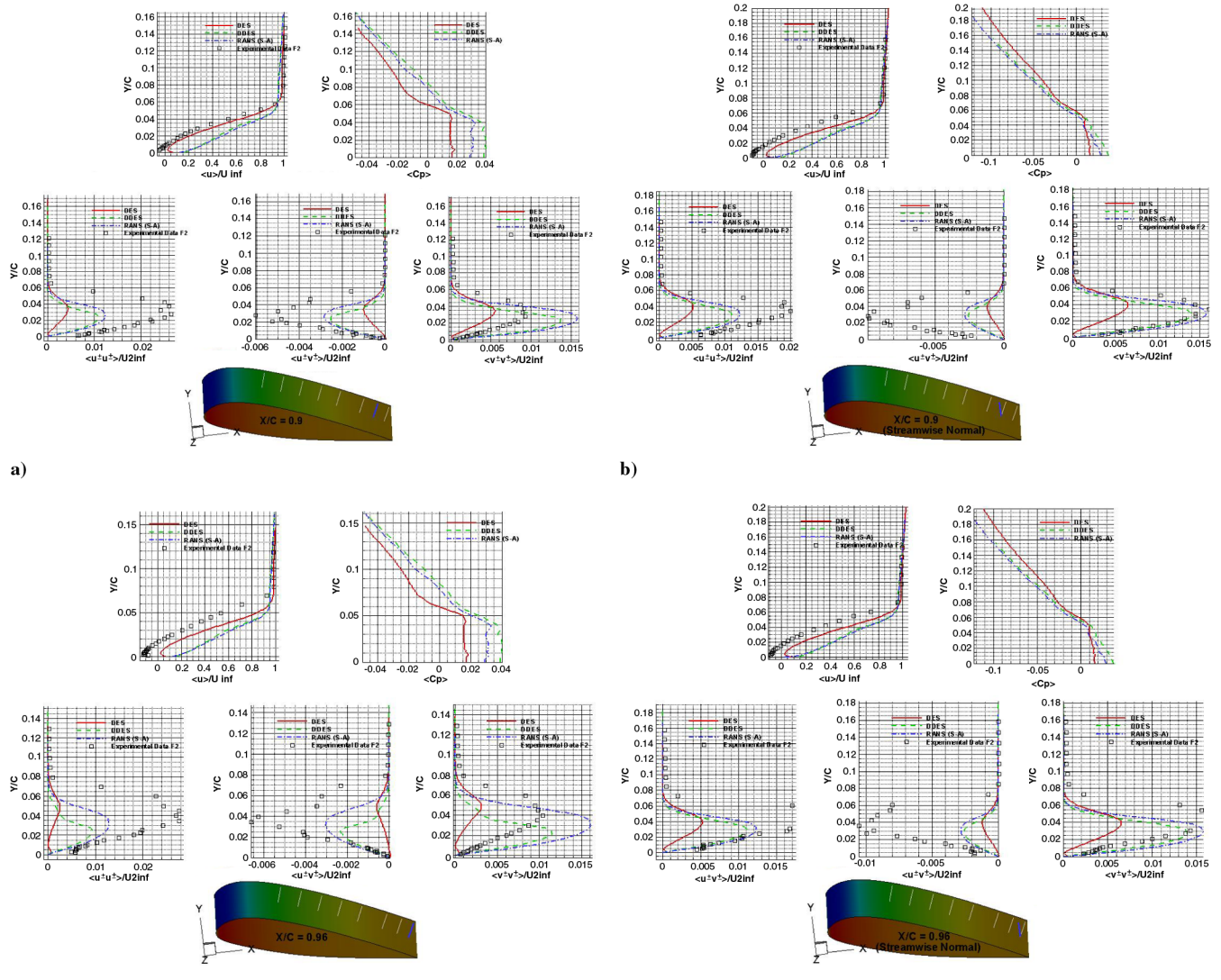

Fig. 11 Comparison of $\langle u\rangle$, modeled Reynolds stresses, and $\langle C_p\rangle$ from RANS, DES, and DDES with experimental data F2: a-f) computed normal to the airfoil surface and g) computed normal to the freestream flow direction at specified location.

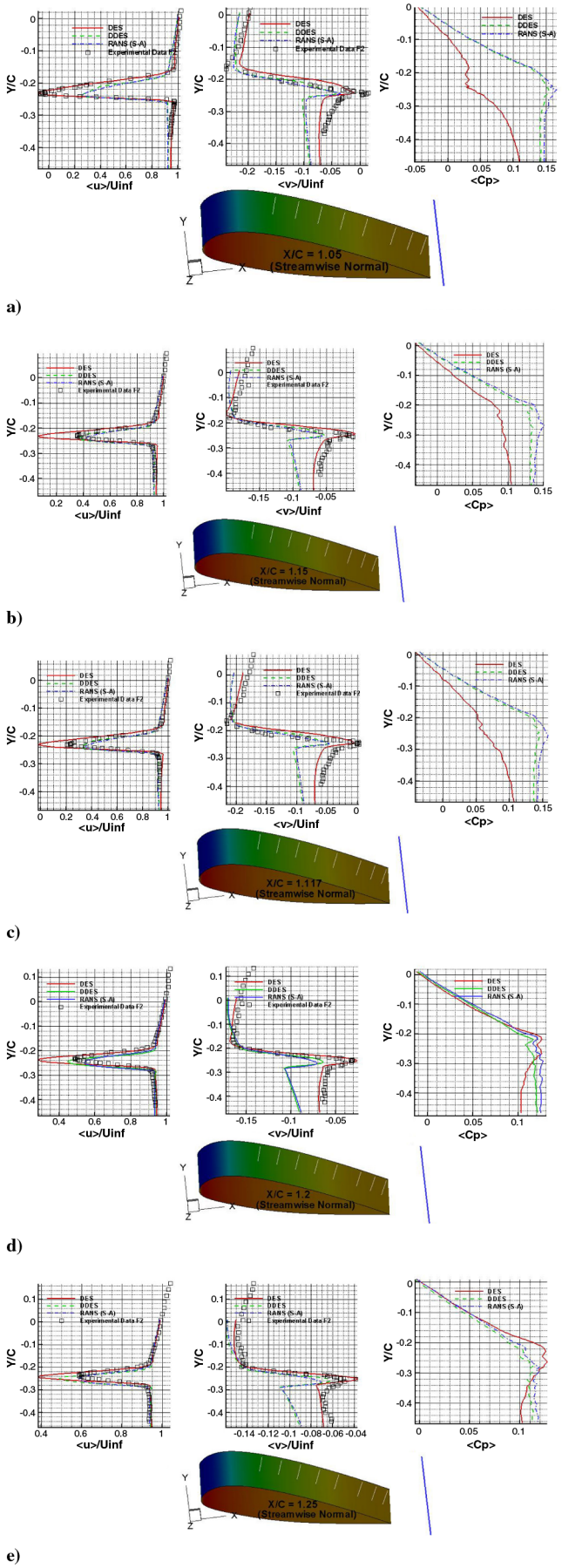

Fig. 12 Comparison of time-averaged $\langle u \rangle$, $\langle v \rangle$, and $\langle C_p \rangle$ from URANS, DES, and DDES with experimental data F2: a–f) computed normal to the airfoil surface and g) computed normal to the freestream flow direction at specified location.

Figures 9a–9c show the contour plots of the turbulent Reynolds stresses over A-airfoil form DES simulation normalized by the square of the inlet velocity with probes for normal to the surface data extraction. It is evident that the high turbulent Reynolds stresses are obtained in the attached boundary-layer region and in the shear layer in the wake region. Figures 10a–10g present the comparison of the turbulent Reynolds stresses at 30–82.5% of the chord on the suction side of the A-airfoil from URANS, DES, and DDES simulations with the experimental data F2 [12]. Experimentally, the boundary-layer separation on the suction side of the A-airfoil occurs just after this region. The results from URANS, DES, and DDES schemes, in general, show that the general trends in the experimental data are correctly predicted. The prediction of x-direction velocity component is slightly lower in the region away from airfoil surface. The reason of presenting $\langle C_p \rangle$ along all the probe lines is to appreciate the difference in the results of URANS and DDES, which is otherwise difficult to note from other plots. All these schemes underpredict the $\langle u'u' \rangle$ and $\langle u'v' \rangle$ turbulent Reynolds stresses and overpredict the $\langle v'v' \rangle$ component. Turbulent Reynolds stresses $\langle u'u' \rangle$, in general, show better agreement as compared with $\langle v'v' \rangle$, and DES has lower prediction as compared with URANS and DDES, understandably due to switching to less dissipative LES mode.

The x-direction velocity is relatively better predicted by the DES simulations from $60\%c$ onward in the downstream direction. Figures 10f and 10g present an interesting comparison. The location for both is the same at $82.5\%c$; however, Fig. 10f is the normal to the airfoil surface and Fig. 10g is the normal to the freestream flow direction, although the turbulent stress $\langle v'v' \rangle$ predicted by the DES in Figure 10f and by DDES in Fig. 10g are quite close the experimental data. However, none of the numerical simulations show the change in the experimental data in this region. It is expected to be due to the presence of a separation bubble or adverse pressure region observed experimentally.

Figures 11a–11d show the comparison of modeled Reynolds stresses computed from the URANS, DES, and DDES schemes with the experimental data F2 [12], and this region is experimentally observed to have a flow separation. The x-direction velocity is better predicted by the DES simulations. However, modeled Reynolds stress predictions with URANS and DDES schemes are closer to those of the experimental data.

Wake-Region Analysis

The wake region is arguably a difficult region to simulate with reasonable accuracy. In particular, the presence of turbulence and separation make it quite challenging to predict the correct flowfield in the wake region.

Figures 12a–12e present the comparison of time-averaged velocity parameters and C_p obtained from URANS, DES, and DDES simulations with the experimental data F2 [12]. The $\langle v \rangle$ velocity computation by the DES simulation is in much better agreement with the experimental data F2, as compared with the URANS and DDES results.

Figure 12a shows a good prediction of $\langle u \rangle$ velocity from DES simulation; however, for locations further downstream, URANS and DDES results are better. The results of $\langle u \rangle$ from URANS and DDES are similar until $1.15c$ (15% chord aft of the trailing edge) in the wake region and are in better agreement with the experimental data as compared with the DES simulation. Further downstream of this point, both DES and DDES overpredict the $\langle u \rangle$ velocity and more dissipative URANS seems to have better agreement with the experimental data.

Conclusions

The numerical studies carried out in this work show that DES simulations may benefit from its premature switching to LES mode for the mild separation cases. The direct application of DDES for mild separation problems can lead to its recovery to URANS solutions, failing to predict the separation totally. The $\langle v \rangle$ velocity prediction in the wake region is well predicted by the DES

simulation, due to its preservation of the separation and unsteadiness in the flow. The modeled Reynolds stresses in the flow computed by using the URANS and DDES simulations are very similar, despite the fact that the surface mean pressure distributions show some small differences. The relative dissipation in URANS in the wake region is higher than that in DDES, as shown in the wake-region analysis of time-averaged x-direction velocity $\langle u \rangle$. The results of DES, especially the velocity predictions in the wake region, are quite encouraging. For the cases where no abrupt massive separation occurs, to be categorized as nonnatural DES cases, the DDES may prove overly dissipative to damp out the unsteadiness in the flow. If the delayed-switching in the RANS region is of such effect that it damps out the natural unsteadiness in the flow, the DDES simulation will not be able to preserve the unsteadiness in the flow domain. For such cases the use of synthetic turbulence [26,27] with the DDES may give better results.

For the flows with mild separation, the application of DDES may prove to be inappropriate, based on the results obtained from this study.

Acknowledgments

The authors gratefully acknowledge the support from the Engineering and Physical Sciences Research Council through the U.K. Applied Aerodynamic Consortium in using the HECToR High Performance Computing System. The first author is funded by a U.K. Overseas Research Scholarship. The partners of the LESFOIL project are acknowledged for sharing their data. The authors also thankfully acknowledge Frank Thiele and Charles Mockett from the Institute of Fluid Mechanics and Engineering Acoustics, Technical University of Berlin, for some helpful discussions.

References

[1] Piomelli, U., and Balaras, E., "Wall-Layer Models for Large-Eddy Simulations," *Annual Review of Fluid Mechanics*, Vol. 34, 2002, pp. 349–374. doi:10.1146/annurev.fluid.34.082901.144919

[2] Dahlstrom, S., and Davidson, L., "Large Eddy Simulation of the Flow Around an Airfoil," 39th AIAA Aerospace Sciences Meeting and Exhibit, AIAA Paper 2001-0425, Reno NV, 8–11 Jan. 2001.

[3] Tannehill, J. C., Anderson D. A., and Pletcher, R. H., *Computational Fluid Mechanics and Heat Transfer*, 2nd ed., Taylor and Francis, London, 1997.

[4] Kim, J., Moin, P., and Moser, R. D., "Turbulence Statistics in Fully Developed Channel Flow at Low Reynolds Number," *Journal of Fluid Mechanics*, Vol. 177, 1987, pp. 133–166. doi:10.1017/S0022112087000892

[5] Spalart, P. R., Jou, W-H., Strelets, M., and Allmaras, S. R., "Comments on the Feasibility of LES for Wings and on a Hybrid RANS/LES Approach," *First AFOSR International Conference on DNS/LES*, Greyden, Columbus, OH, 4–8 Aug. 1997.

[6] Menter, F. R., and Kuntz, M., "Adaptation of Eddy Viscosity Turbulence Models to Unsteady Separated Flow Behind Vehicles," *Aerodynamics of Heavy Vehicles: Trucks, Busses, and Trains*, edited by R. McCallen, F. Browand, and J. Ross, Springer, Berlin, 2004.

[7] Spalart, P., Deck, S., Shur, M., Squires, K., Strelets, M. K., and Travin, A., "A New Version of Detached-Eddy Simulation, Resistant to Ambiguous Grid Densities," *Theoretical and Computational Fluid Dynamics*, Vol. 20, July 2006, pp. 181–195. doi:10.1007/s00162-006-0015-0

[8] Spalart P. R., "Detached-Eddy Simulation," *Annual Review of Fluid Mechanics*, Vol. 41, 2009, pp. 181–202. doi:10.1146/annurev.fluid.010908.165130

[9] Davidson, L., "LESFOIL: A European Project on Large Eddy Simulations Around a High-Lift Airfoil at High Reynolds Number," *Proceedings of ECCOMAS 2000*, Barcelona, 11–14 Sept. 2000.

[10] Mellen, C. P., "Lessons from the European LESFOIL Project on LES of Flow Around an Airfoil," 40th AIAA Aerospace Sciences Meeting and Exhibit, AIAA Paper 2002-0111, Reno, NV, Jan. 2002.

[11] Mellen, C. P., Frohlich, J., and Rodi, W., "Lessons from LESFOIL Project on Large-Eddy Simulation of Flow Around an Airfoil," *AIAA Journal*, Vol. 41, No. 4, April 2003, pp. 573–581. doi:10.2514/2.2005

[12] Gleyzes, C., "Operation Decrochage—Resultats de la 2eme Campagne d'Essais a F2- Mesures de Pression et Velocimetrie Laser," ONERA, TR RT-DERAT 55/5004, 1989.

[13] Cokljat, D., and Liu, F., "DES of Turbulent Flow over an Airfoil at High Incidence," 40th Aerospace Sciences Meeting and Exhibit, AIAA Paper 2002-0590, Reno, NV, 14–17 Jan. 2002.

[14] Schmidt, S., and Thiele, F., "Detached Eddy Simulation of Flow Around A-Airfoil," *Flow, Turbulence and Combustion*, Vol. 71, 2003, pp. 261–278. doi:10.1023/B:APPL.0000014933.66058.22

[15] Qin, N., and Xia, H., "Detached Eddy Simulation of a Synthetic Jet for Flow Control," *Proceedings of the Institution of Mechanical Engineers, Part I (Journal of Systems and Control Engineering)*, Vol. 222, No. 5, 2008, pp. 373–380. doi:10.1243/09596518JSCE513

[16] Durrani, N. I., "Hybrid RANS-LES Simulations for Separated Flows Using Dynamic Grids," Ph.D. Thesis, Univ. of Sheffield, Sheffield, England, U.K., March 2009.

[17] Spalart, P. R., and Allmaras, S. R., "A One-Equation Turbulence Model for Aerodynamic Flows," AIAA Paper 92-0439, Jan. 1992.

[18] Shur, M., Spalart, P. R., Strelets, M., and Travin, A., "Detached-Eddy Simulation of an Airfoil at High Angle of Attack," *Proceedings of the 4th International Symposium on Engineering Turbulence Modelling and Measurements*, Elsevier, Amsterdam, 24–26 May 1999, pp. 669–678.

[19] Spalart, P., Deck, S., Shur, M., Squires, K., Strelets, M. K., and Travin, A., "A New Version of Detached-Eddy Simulation, Resistant to Ambiguous Grid Densities," *Theoretical and Computational Fluid Dynamics*, Vol. 20, July 2006, pp. 181–195. doi:10.1007/s00162-006-0015-0

[20] Roe, P. L., "Approximate Riemann Solvers, Parameters Vectors and Difference Schemes," *Journal of Computational Physics*, Vol. 43, 1981, pp. 357–372. doi:10.1016/0021-9991(81)90128-5

[21] Weiss, J. M., and Smith, W. A., "Preconditioning Applied to Variable and Constant Density Flows," *AIAA Journal*, Vol. 33, No. 11, 1995, pp. 2050-2057. doi:10.2514/3.12946

[22] Pandya, A. S., Venkateswaran, S., and Pulliam, H. T., "Implementation of Preconditioned Dual-time Procedures in OVERFLOW," 41st AIAA Aerospace Sciences Meeting and Exhibit, Reno, NV, AIAA Paper 2003-0072, Jan. 2003.

[23] Wilcox, D. C., "Turbulence Modeling for CFD," 2nd ed., DCW Industries, La Cañada, CA, 1998.

[24] Bradshaw, P., Ferriss, D. H., and Atwell, N. P., "Calculation of Boundary-Layer Development Using the Turbulent Energy Equation," *Journal of Fluid Mechanics*, Vol. 28, No. 3, 1967, pp. 593–616. doi:10.1017/S0022112067002319

[25] Townsend, A. A., *The Structure of Turbulent Shear Flow*, Cambridge Univ. Press, New York, 1956.

[26] Keating, A., De Prisco, G., and Piomelli, U., "Interface Conditions for Hybrid RANS/LES Calculations," *International Journal of Heat and Fluid Flow*, Vol. 27, 2006, pp. 777–788. doi:10.1016/j.ijheatfluidflow.2006.03.007

[27] De Prisco, G., Piomelli, U., and Keating, A., "Improved Turbulence Generation Techniques for Hybrid RANS/LES Calculations," *Journal of Turbulence* [online journal], Vol. 9, No. 5, 2008. doi:10.1080/14685240701787744